

Structure of fast-ion-conducting AgI-doped borate glasses in bulk and thin film forms

C. P. Varsamis, E. I. Kamitsos,* and G. D. Chryssikos

Theoretical and Physical Chemistry Institute, National Hellenic Research Foundation, 48 Vassileos Constantinou Avenue, Athens 116 35, Greece

(Received 17 November 1998)

The reflectance spectra of bulk superionic glasses $x\text{AgI}-(1-x)[\text{Ag}_2\text{O}-n\text{B}_2\text{O}_3]$ with $n=2$, $0 \leq x \leq 0.65$ (diborate) and $n=0.5$, $0.40 \leq x \leq 0.60$ (pyroborate) have been measured in the infrared to investigate the structure of the boron-oxygen network and the nature of sites hosting silver ions. The analysis of the mid-infrared spectra showed that the diborate network consists of borate triangles BO_3 and $\text{B}\text{O}_2\text{O}^-$, and borate tetrahedra BO_4^- (O =oxygen atom bridging two boron centers). Similarly, it was shown that pyroborate dimers $\text{B}_2\text{O}_5^{4-}$, orthoborate monomers BO_3^{3-} , and borate tetrahedra constitute the short-range order of pyroborate glasses. The relative abundance of these borate units was found to be affected by AgI doping in a way that can be described by the isomerization reaction $\text{B}\text{O}_2\text{O}^- \rightleftharpoons \text{B}\text{O}_4^-$ for $n=2$ and the disproportionation reaction $\text{B}_2\text{O}_5^{4-} \rightleftharpoons \text{BO}_3^{3-} + \text{B}\text{O}_4^-$ for $n=0.5$. Both reactions shift to the right upon increasing the amount of AgI. This influence of the doping salt on the glass structure causes the lowering of the glass transition and fictive temperature at which the structure of the supercooled liquid is frozen into the glassy state. A parallel study of infrared transmission spectra of thin films in the diborate family showed the presence of a background interference wave that affects strongly the relative intensity of bands due to borate tetrahedra and triangular units. This finding suggests that conclusions based on direct comparison of infrared spectra of thin film and bulk samples of the same composition should be drawn with caution. The study of the far-infrared profiles of glasses in the pyroborate series suggested that the majority of silver ions exist in two distributions of coordination environments; one is formed primarily by oxygen atoms provided by the borate network and the other is made mainly by iodide ions, without excluding the presence of mixed oxyiodide sites. The spectroscopic characteristics of silver iodide sites were found to change progressively with AgI addition and to point towards sites of tetrahedral coordination such as those found in crystalline AgI. However, for diborate glasses the far-infrared results suggest the presence of oxide, iodide, and mixed O/I environments for silver ions. Therefore, this study shows that the formation and organization of separate silver iodide sites in $x\text{AgI}-(1-x)[\text{Ag}_2\text{O}-n\text{B}_2\text{O}_3]$ glasses depends on both Ag_2O and AgI content. [S0163-1829(99)02030-5]

I. INTRODUCTION

Fast-ion-conducting (FIC) glasses comprise a class of solid electrolytes which have been attracting much attention for their potential applications to solid-state electrochemical devices, including batteries, sensors, and electrochromic displays.¹⁻³ Because of their technological importance, FIC glasses have been investigated extensively to establish the chemical and structural characteristics responsible for their high ionic conductivity. The acquisition of this knowledge is critical not only for explaining the mechanism of ion transport in glass, but also for designing systems with improved performance appropriate for the current needs.¹⁻⁸

The composition of oxide-based FIC glasses can be expressed as $z\text{MX}-(1-z)[\text{M}_2\text{O}-n\text{F}_x\text{O}_y]$ where M is a univalent metal, usually Li, Na, Ag, and Cu and the halogen X is I, Br, or Cl. The Lewis acid F_xO_y is a glass-forming (e.g., B_2O_3 , P_2O_5 , SiO_2 , and GeO_2) or other (MoO_3 , WO_3) oxide. The large body of conductivity data on ion-conducting glasses accumulated over the past two decades suggests some empirical relations between ionic conductivity and glass composition. Thus it is known that ionic conductivity is enhanced by orders of magnitude upon increasing the concentration of the metal-oxide modifier and the metal-halide doping salt.⁹⁻¹⁵ Even higher conductivity can be achieved by combining a relatively small and polarizable metal ion (e.g.,

Ag^+ , Cu^+) with the large and polarizable iodide ion I^- .^{16,17} Further improvement of conductivity can be obtained by mixing two glass-forming oxides, a phenomenon known as the mixed-anion or mixed-glass former effect.^{18,19} Finally, replacement of oxygen by sulfur or selenium leads to the formation of FIC chalcogenide glasses with conductivities exceeding those of the corresponding oxide glasses by three orders of magnitude or more.²⁰⁻²² Proper optimization of the above chemical factors has resulted in the synthesis of new FIC glasses in the system



where the ionic conductivity reaches the value of $4 \times 10^{-2} (\Omega \text{ cm})^{-1}$ at room temperature for the composition $z=0.4$.²³

Despite the numerous experimental and theoretical studies devoted to FIC glasses, the structure and the ion conduction mechanism are still a matter of debate.⁶⁻⁸ Even for the ‘‘simpler’’ binary glasses $\text{M}_2\text{O} \cdot n\text{F}_x\text{O}_y$, a range of models has been proposed to explain the ion diffusion mechanism. It includes the strong electrolyte model,²⁴ the weak electrolyte model,^{25,26} the modified random network model,²⁷ the jump diffusion model,²⁸ and the dynamic structure model.^{29,30} The use of a doping salt as a third component of the glass complicates even more the situation. As a result, there is no con-

sensus for the state of the doping salt in the glass matrix and its role in the ion transport process. One model proposes the formation of a structurally inhomogeneous glass where MX (mainly AgI) forms microdomains or clusters within the host matrix.^{31–35} Movement of silver ions is thought to be facilitated by the formation of conducting pathways along the AgI microdomains.² A second model suggests that AgI is highly dispersed in interstices or voids controlled by oxygen atoms of the host matrix and that AgI enhances ionic conductivity by lowering the potential energy barriers within the glass.^{36–38} Other authors emphasize the role of the doping salt in expanding the glass network and creating larger doorways between sites of mobile ion.³⁹ In fact, a scaling relation between conductivity enhancement and the expansion of the network-forming units was found to operate in MX -doped borate and phosphate glasses.⁴⁰ Thus, while it may appear that the details of the glass structure have no direct effect on ionic conductivity, it is the interactions at the local- and intermediate-range order that control the degree of expansion of the glass network.

Glasses in the $x\text{AgI}-(1-x)[\text{Ag}_2\text{O}-n\text{B}_2\text{O}_3]$ system were prepared by Magistris *et al.*^{11,12} and Minami *et al.*,^{13–15} and received subsequently particular attention as model systems of FIC glasses. The special interest in these glasses is due to the fact that they are stable, with relatively high glass transition temperature, high ionic conductivity, and can be prepared easily in a wide glass-forming region. This is achieved by varying the doping salt, AgI, content (x) and/or the modifier oxide, Ag_2O content (n). Besides their high ionic conductivity, compositions in this glass system were found recently to exhibit interesting nonlinear optical properties.⁴¹

Early investigations of AgI-borate glasses by Minami *et al.*,^{14,15} employing infrared (IR) transmission spectroscopy on thin blown films, showed that the short-range order (SRO) of the borate network depends directly on the AgI content, despite the fact that the $\text{Ag}_2\text{O}/\text{B}_2\text{O}_3$ ratio was kept fixed. In particular, it was found that as the AgI content in the glass increases, the intensity of the absorption band due to boron-oxygen tetrahedral units increases also relative to that of the band due to boron-oxygen triangular units. On the contrary, Chiodelli *et al.*⁴² studied the same system by ¹¹B NMR and IR spectroscopy and concluded that AgI is dispersed in interstices and has only minor effects on the short-range order of the borate network. The model of dispersed AgI in borate glasses is supported also by results of ¹⁰⁹Ag NMR,³⁸ extended x-ray absorption fine structure (EXAFS),⁴³ and x-ray diffraction⁴⁴ investigations. Contrary to this picture, Raman^{32,45} and infrared^{46–48} spectroscopic investigations provide evidence for the development of disordered AgI microdomains upon increasing the silver iodide content. It is interesting to note that, although the IR results obtained from the analysis of reflectance spectra of bulk glasses^{46,47} demonstrate that the effect of AgI on the SRO is similar to that reported by Minami *et al.*,^{14,15} an IR transmission study of the corresponding glass compositions in thin film forms indicates that the short-range structure remains unaffected by AgI.⁴⁸ Such variations in the IR results were attributed⁴⁸ to the different preparation methods used in different studies, since the source of the silver oxide modifier can be either pure Ag_2O (Refs. 14, 15, 46, and 47) or AgNO_3 .⁴⁸

Heat capacity measurements of AgI-borate glasses with $n \approx 1$ and $x \approx 0.5$ revealed the presence of a β transition in the liquid-nitrogen temperature region. This transition was attributed to the freezing-in of the rearrangement of silver ions in amorphous AgI aggregates.⁴⁹ Recently, Tatsumisago *et al.*⁵⁰ performed field emission scanning electron microscopy in twin-roller-quenched $0.75\text{AgI}-0.25[\text{Ag}_2\text{O}-0.33\text{B}_2\text{O}_3]$ glass and reported the presence of AgI-rich amorphous particles (40–60 nm in diameter) at ambient temperature. Annealing this glass at 120 °C, or increasing the AgI content to 80 mol %, was found to cause the aggregation of these AgI-rich amorphous particles into island regions, which were several hundreds of nanometers in size, and appeared decorated by a fine dispersion of α -AgI particles 20–30 nm in size.

In addition to the above, the AgI-diborate system ($n = 2$) was studied recently by neutron and x-ray diffraction techniques, and the experimental data were used to construct structural models using the reverse Monte Carlo method.⁵¹ The authors of this work concluded that, while the SRO of the borate network is unaffected by AgI doping, increasing the amount of AgI improves the medium-range order (MRO) of the glass by inducing ordering between the neighboring boron-oxygen chain segments. It was therefore proposed that the improvement of MRO in glass could be connected with the network expansion and the creation of new pathways for ion transport. The idea of network expansion by AgI doping is supported also by results of a parallel analysis of x-ray and neutron diffraction data on diborate ($n = 2$) and tetraborate ($n = 4$) glasses.^{52,53} However, Cervinka *et al.* attributed this network expansion to the formation of organized AgI-rich regions, which develop between the boron-oxygen configurations and separate them by greater distances.^{52,53}

The existing diversity of viewpoints regarding the details of the glass structure and the ways it is affected by AgI doping suggests that further work is required for a better understanding of the AgI-borate model system. Continuing our studies on fast-ion-conducting glasses,^{46,47} we report in this paper results of an infrared investigation of glasses in the system $x\text{AgI}-(1-x)[\text{Ag}_2\text{O}-n\text{B}_2\text{O}_3]$ with $n = 2$ (diborate) and $n = 0.5$ (pyroborate) and with AgI contents spanning the ranges $0 \leq x \leq 0.65$ for $n = 2$ and $0.40 \leq x \leq 0.60$ for $n = 0.5$. To resolve the origin of the discrepancies found in some of the previous infrared reflectance^{46,47} and transmittance⁴⁸ investigations, AgNO_3 was used as the source of Ag_2O and the glasses were prepared in the form of both bulk samples and thin films, whenever this was possible. The infrared spectra were measured in a broad frequency range (30–4000 cm^{-1}) using the techniques of specular reflectance and transmission for bulk samples and thin films, respectively. The two sets of spectral data were analyzed to yield information on the short-range order of the borate arrangements that form the glass network and on the nature of sites occupied by silver ions. The results from bulk glasses and thin films are compared and discussed in relation to previous infrared findings and models proposed for AgI-containing borate glasses.

II. EXPERIMENT

A. Glass preparation

Glasses in the system $x\text{AgI}-(1-x)[\text{Ag}_2\text{O}-n\text{B}_2\text{O}_3]$ ($n = 2, 0.5$) were prepared from reagent-grade AgI, AgNO_3 ,

and B_2O_3 . Stoichiometric amounts of the dry reagents were weighed, thoroughly mixed, and ground to form batches corresponding to ca 5 g of glass. The batches were placed in uncovered Pt crucibles and transferred in an electrically heated furnace at 650 °C. After the evolution of nitrogen oxides had ceased the temperature was raised slowly to 850–950 °C and the melt remained in the furnace for an additional 20–30 min depending on composition. The melt was stirred frequently to ensure homogeneity.

Part of the melt was splat quenched between two polished copper blocks to yield clear bulk samples. These specimens were in the form of ~1-mm-thick disks with good surfaces and were used for reflectance measurements without any further treatment. By using the splat quenching method, glasses could be prepared continuously in the composition ranges $0 \leq x \leq 0.65$ for the diborate family and $0.40 \leq x \leq 0.60$ for the pyroborate family.

For glasses in the diborate series, attempts were made to prepare also thin films from the remaining of the melt, following the procedure described by Liu and Angell.⁵⁴ After removing the crucible from the furnace, a 5-mm-diam Pyrex tube was used to attach a small viscous droplet from the melt surface. A few seconds later, dry nitrogen was admitted to the tube to produce a glass bubble from which thin films were collected. Depending on the viscosity of the melt droplet and the pressure of nitrogen gas, films of different thickness could be prepared from the same batch composition. This technique resulted in clear films when the melt composition was in the range $0.1 \leq x \leq 0.60$, but failed to yield films for the binary glass ($x=0$) and the composition with the highest AgI content ($x=0.65$), for which glasses were obtained only by splat quenching.

B. Infrared measurements

Infrared spectra were measured at room temperature on a Fourier-transform vacuum spectrometer (Bruker 113v), properly equipped with sources (Hg arc and global) and detectors (DTGS with KBr and polyethylene windows) to allow coverage in the far-infrared ($<700 \text{ cm}^{-1}$) and midinfrared ($400\text{--}5000 \text{ cm}^{-1}$) regions. For this purpose, five Mylar beam splitters of different thickness ($3.5\text{--}50 \mu\text{m}$) were used for far-infrared measurements and a KBr beam splitter was used in the mid-IR. Therefore, for each sample six different spectra were measured and the optimum beam splitter throughputs were finally merged into one data file to give a continuous spectrum in the range $25\text{--}5000 \text{ cm}^{-1}$. Each spectrum represents the average of 200 scans at 2 cm^{-1} resolution.

Specular reflectance measurements on bulk samples were made in a quasinormal incidence mode (11°) using an aluminum mirror as reference, while for transmittance measurements the plane of the film was oriented perpendicular to the incident beam. Free-standing films with dimensions greater than approximately $1 \text{ cm} \times 1 \text{ cm}$ were mounted directly on the sample holder. Smaller films, having areas larger than the cross section of the infrared beam, were sandwiched between two dry KBr windows suitable for infrared measurements. In the latter case the spectra were measured in the mid-IR range allowed by the KBr window ($600\text{--}5000 \text{ cm}^{-1}$). To prevent hydrolysis and photodecomposition the infrared spectrum of

each sample, prepared by either technique, was measured immediately after its formation.

C. Data analysis

The specular reflectance spectra $R(\nu)$ of bulk samples can be analyzed either by the Kramers-Kronig (KK) transformation or by the curve-fitting procedure using the classical dispersion theory to model the dielectric function. In recent studies of ionic glasses, we have shown that both procedures lead to almost identical results.^{55,56} In this work we have performed the KK analysis to obtain the frequency-dependent optical and dielectric properties of glasses, and present the results in the absorption coefficient formalism that permits comparison with published data. The absorption coefficient spectra $\alpha(\nu)$ were calculated from the expression

$$\alpha(\nu) = 4\pi\nu k(\nu), \quad (1)$$

where ν is the frequency in cm^{-1} and $k(\nu)$ is the imaginary part of complex refractive index, $\tilde{n}(\nu) = n(\nu) - ik(\nu)$. Due to the amorphous nature of the samples, the infrared bands are very broad and any further analysis of the absorption coefficient spectra requires spectral deconvolution into component bands.⁵⁷ In this study, the absorption coefficient spectra were deconvoluted into Gaussian components according to the relation

$$\alpha(\nu) = \sum_j \alpha_j e^{-2(\nu - \nu_j)^2 / \Delta \nu_j^2}, \quad (2)$$

where each component band is characterized by the resonance frequency ν_j , the bandwidth $\Delta \nu_j$, and the value of the absorption coefficient at the resonance frequency, α_j . The integrated intensity A_j of the j th component band was calculated by

$$A_j = \int_{-\infty}^{\infty} \alpha_j e^{-2(\nu - \nu_j)^2 / \Delta \nu_j^2} d\nu = \sqrt{\pi/2} \Delta \nu_j \alpha_j. \quad (3)$$

For the transmittance spectra of thin films, the KK analysis is no longer valid due to multiple internal reflections inside the film. In order to simulate the experimental transmittance spectrum $T(\nu)$ of a finite film with thickness t , we have employed the following exact expression⁵⁸ which takes fully into account the contribution of the multiple reflections inside the film:

$$T(\nu, n, k, t) = \frac{[1 + R^2 - 2 \text{Re}(r^2)]D}{A + B \cos 2\theta + C \sin 2\theta}, \quad (4)$$

where

$$r = |r| e^{i\varphi} = \frac{1 - n + ik}{1 + n - ik}, \quad (4a)$$

$$R = |r|^2 = \frac{(1 - n)^2 + k^2}{(1 + n)^2 + k^2}, \quad (4b)$$

$$D = e^{-\alpha t}, \quad (4c)$$

$$A = 1 + R^2 D^2, \quad (4d)$$

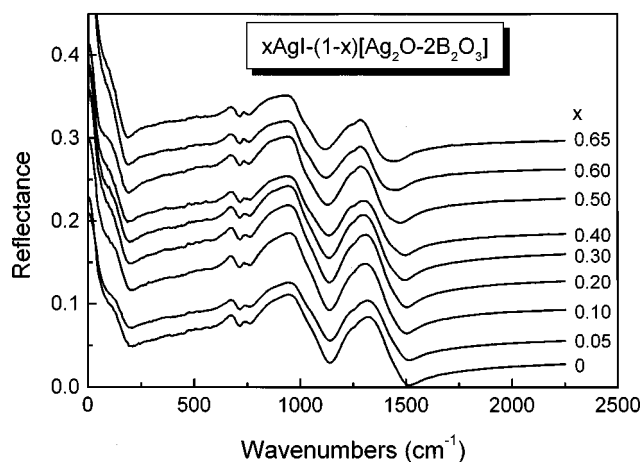


FIG. 1. Infrared reflectance spectra of AgI-containing diborate glasses, $x\text{AgI}-(1-x)[\text{Ag}_2\text{O}-2\text{B}_2\text{O}_3]$. The spectra have been offset by 0.03 to allow comparison.

$$B = -2RD \cos 2\varphi, \quad (4e)$$

$$C = -2R \sin 2\varphi, \quad (4f)$$

$$\theta = 2\pi\nu nt. \quad (4g)$$

In the above expressions the frequency dependence of n , k , and α has been omitted for convenience. The experimental transmittance spectra were fitted by using Eq. (4) and employing as input the $n(\nu)$ and $k(\nu)$ spectra calculated by the KK analysis of the bulk samples prepared from the same batch. Therefore, the only adjustable parameter in the fitting procedure is the thickness of the film. It can be shown that the transmittance spectra calculated through Eq. (4) contain interference fringes with spacing δ in frequency equal to $1/2nt$.

III. RESULTS

A. Infrared spectra of bulk samples

Typical reflectance spectra of bulk samples are shown in Fig. 1 for glasses in the diborate series starting from the binary glass ($x=0$) and having AgI contents as high as $x=0.65$. Despite the large range of AgI contents covered in this study, it is observed that all reflectance curves have quite similar bandshapes. Nevertheless, some systematic variations in relative band intensities with addition of AgI can be observed in the reflectance spectra of Fig. 1 and manifest themselves in corresponding changes of the absorption coefficient (AC) spectra. The latter were obtained by the KK analysis of the reflectance spectra and are depicted in Fig. 2. In the far-IR region the absorption spectra show the presence of a weak band below 200 cm^{-1} , which can be attributed to the localized rattling motion of Ag^+ ions in their hosting sites.^{46,47} The changes induced in the AC spectra with increasing amount of AgI include the increase of the intensity of the absorption envelope centered at ca 1000 cm^{-1} relative to that of the envelope at ca 1350 cm^{-1} and the systematic narrowing of the latter.

Previous studies of alkali and silver borate glasses with metal oxide contents below the metaborate composition (50

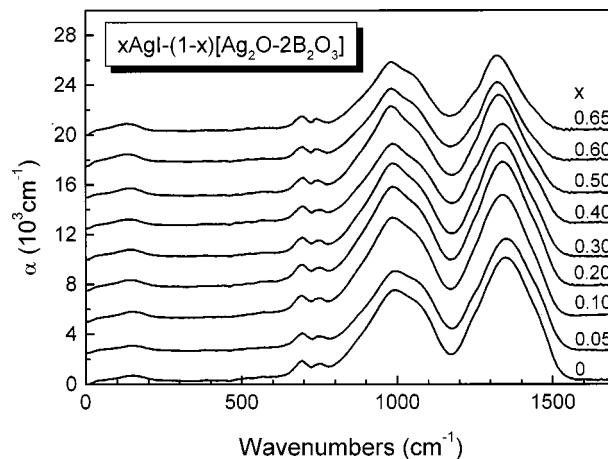


FIG. 2. Absorption coefficient spectra of $x\text{AgI}-(1-x)[\text{Ag}_2\text{O}-2\text{B}_2\text{O}_3]$ glasses calculated by Kramers-Kronig transformation of the reflectance spectra. The spectra have been offset by $2.5 \times 10^3\text{ cm}^{-1}$ to allow comparison.

mol % $M_2\text{O}$) have shown that the complex envelope peaking at ca 1000 cm^{-1} can be attributed to the asymmetric stretching vibration of boron-oxygen bonds in borate tetrahedra, BO_4^- (O =oxygen atom bridging two boron atoms).^{59,60} The high-frequency envelope at ca 1300 cm^{-1} is assigned to the corresponding vibration in borate triangles. For silver-borate glasses with Ag_2O contents up to 33 mol %, there are two kinds of borate triangles: those having all oxygen atoms of the bridging type, BO_3 , and those with two bridging and one nonbridging oxygen atom, $\text{B}\text{O}_2\text{O}^-$.⁶⁰ The deformation modes of the various borate species give rise to weak infrared bands below 800 cm^{-1} .

The integrated absorption of the AC envelopes between 780 and 1180 cm^{-1} (A_4) and between 1180 and 1570 cm^{-1} (A_3) was calculated to probe the relative population of borate tetrahedra (BO_4^-) and triangles (BO_3 and $\text{B}\text{O}_2\text{O}^-$), respectively, in AgI-containing diborate glasses. The A_4/A_3 ratio depicted in Fig. 3 demonstrates a rather complex dependence on the doping salt content. In the ranges $0 < x < 0.1$ and $0.4 < x \leq 0.65$, the ratio of integrated intensities increases with AgI content, but remains constant within experimental error for compositions $0.1 \leq x \leq 0.4$. It is noted that the A_4/A_3 ratio of glasses prepared previously using Ag_2O (Ref. 47) was found to exhibit a stronger dependence on AgI content than that deduced in the present study for glasses prepared from AgNO_3 . This difference may be attributed to the presence of colloidal silver in the former glasses^{48,61} that could affect the IR reflectivity background and consequently the base line of the absorption spectra.

The absorption coefficient spectra of pyroborate glasses ($n=0.5$) were calculated from the reflectance spectra by the KK transformation and are shown in Fig. 4. The absorption region of borate tetrahedra is dominated by strong bands at ca 955 and 1030 cm^{-1} , while the presence of borate triangles is manifested by features at ca 1245 and 1315 cm^{-1} ($x=0.4$). Comparison with the IR spectra of alkali borate glasses and crystals^{59,62} of high metal oxide content (above 50 mol %) suggests that the band at ca 1240 cm^{-1} can be assigned to the asymmetric stretching vibration of borate triangles with all oxygen atoms being nonbridging, BO_3^{3-}

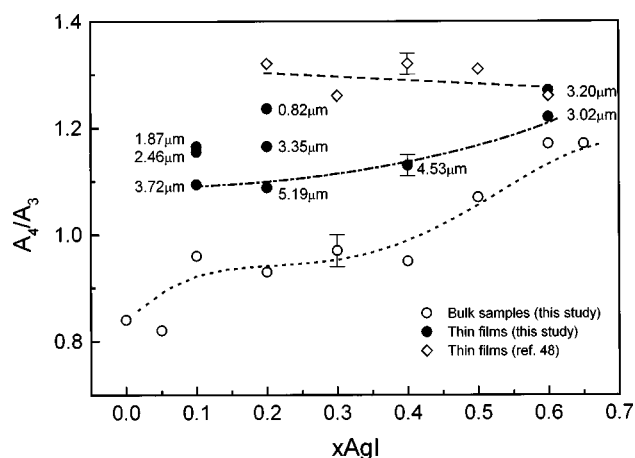


FIG. 3. Dependence of the integrated relative absorption A_4/A_3 on the AgI mole fraction in $x\text{AgI}-(1-x)[\text{Ag}_2\text{O}-2\text{B}_2\text{O}_3]$ glasses. Integrated absorptions A_4 and A_3 correspond to tetrahedral and triangular borate units, respectively. Open and solid circles represent data obtained by the present analysis of absorption coefficient spectra of bulk samples and transmittance spectra of thin films, respectively. Numbers next to thin film data represent the film thickness obtained by the fitting procedure [Eq. (4)]. Thin film data by Hudgens and Martin (Ref. 48) are included for comparison (open diamonds). Lines are drawn to guide the eye.

(orthoborate). Similarly, the band at ca 1315 cm^{-1} can be attributed to the stretching vibration of terminal $\text{B}-\text{O}^-$ bonds of pyroborate dimers, $\text{B}_2\text{O}_5^{4-}$. The latter species give also an IR band in the range $850-1150\text{ cm}^{-1}$ due to the asymmetric stretching vibration of the bridging $\text{B}-\text{O}-\text{B}$ bond. The frequency of this band depends on the mass of the charge-balancing cation and its intensity is approximately equal to that of the characteristic band of terminal $\text{B}-\text{O}^-$ bonds of $\text{B}_2\text{O}_5^{4-}$.⁵⁹ Thus consideration of the IR spectra of Fig. 4 shows that (a) the borate triangles in the pyroborate family are of different nature compared to those found in the diborate family, and (b) the $800-1150\text{ cm}^{-1}$ absorption region contains contributions from both BO_4^- tetrahedra and $\text{B}_2\text{O}_5^{4-}$ species. This indicates that the ratio of integrated

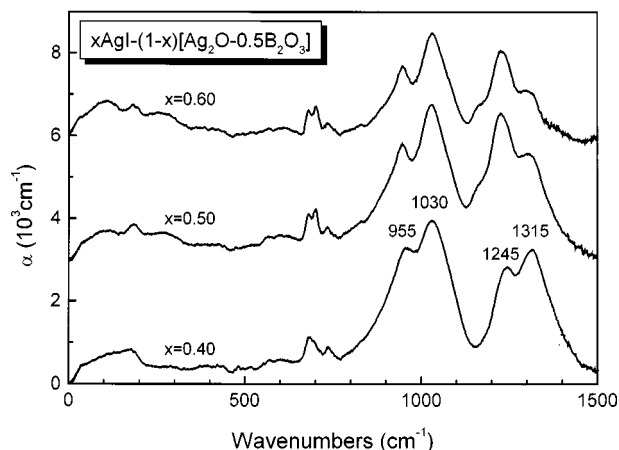


FIG. 4. Absorption coefficient spectra of glasses in the pyroborate series, $x\text{AgI}-(1-x)[\text{Ag}_2\text{O}-0.5\text{B}_2\text{O}_3]$, calculated by Kramers-Kronig transformation of the reflectance spectra. The spectra have been offset by $3 \times 10^3\text{ cm}^{-1}$ to allow comparison.

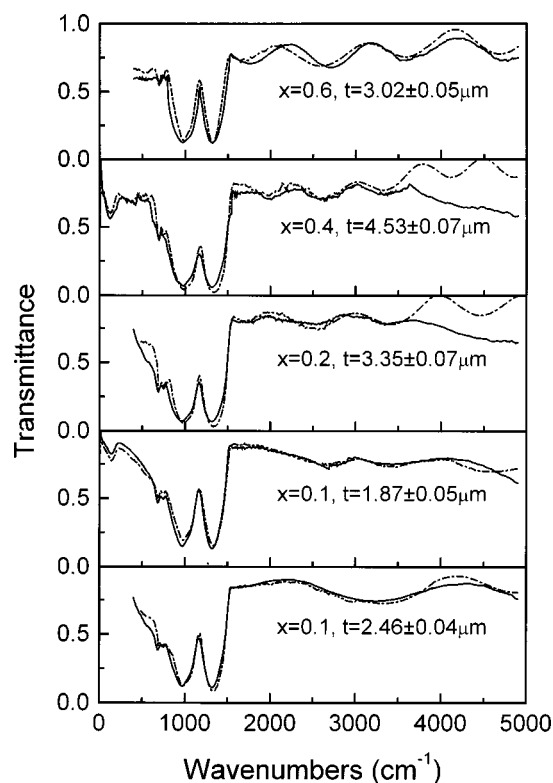


FIG. 5. Typical infrared transmission spectra of films with different AgI contents in the diborate family, $x\text{AgI}-(1-x)[\text{Ag}_2\text{O}-2\text{B}_2\text{O}_3]$. Solid lines indicate experimental spectra of free-standing films ($30-5000\text{ cm}^{-1}$), or films pressed between IR-grade KBr windows ($600-5000\text{ cm}^{-1}$). Dash-dotted lines are the best fits of Eq. (4) to the experimental spectra. The thickness of films obtained by the fitting procedure is also given.

intensities, A_4/A_3 , can not be used in a straightforward way, as in the case of diborates, to quantify the effect of AgI on the glass structure. Nevertheless, it is observed in Fig. 4 that the relative intensity of at least the 1240 and 1315 cm^{-1} bands varies with AgI content, demonstrating the effect of AgI on borate speciation.

B. Infrared spectra of thin films

Infrared transmittance spectra of thin films are shown in Fig. 5 for glasses in the diborate family having AgI contents $x=0.1, 0.2, 0.4$, and 0.6 , and in Fig. 6 for films having a fixed composition ($x=0.2$) but different thickness. All spectra exhibit strong band envelopes at ca 1000 and 1350 cm^{-1} , in agreement with the absorption coefficient spectra resulting from analysis of the reflectance spectra. In addition, interference patterns are present in the transmittance spectra and these are particularly visible in the region above 1500 cm^{-1} where absorption is very small (see Figs. 1 and 2).

Each experimental transmittance spectrum was fitted by means of Eq. (4) using the $n(\nu)$ and $k(\nu)$ spectra of the corresponding bulk sample. The results of fitting are shown in Figs. 5 and 6 and demonstrate a satisfactory agreement with the measured spectra. The value of film thickness t obtained by the fitting procedure is given also in Figs. 5 and 6. An alternative way to calculate film thickness is directly from the interference pattern of the measured transmittance spectrum using the expression

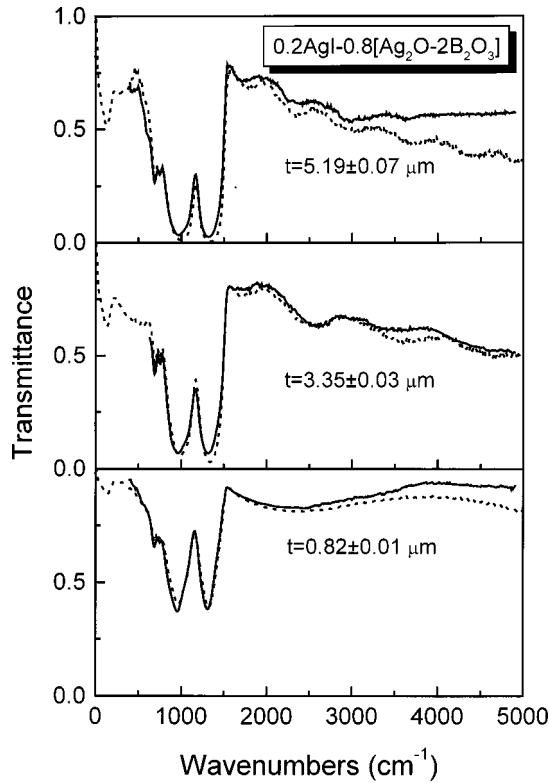


FIG. 6. Effect of film thickness on the transmittance spectra of $x\text{AgI}-(1-x)[\text{Ag}_2\text{O}-2\text{B}_2\text{O}_3]$ glasses. Solid lines are the experimental spectra of films pressed between IR-grade KBr windows, and dotted lines are the best fits of Eq. (4) to the experimental spectra. The thickness of films obtained by the fitting procedure is also given.

$$t = \frac{N}{2[n(\nu_1)\nu_1 - n(\nu_2)\nu_2]}, \quad (5)$$

where N is the number of oscillations between two extrema ($N=1$ for two consecutive maxima or minima) and ν_1 , $n(\nu_1)$ and ν_2 , $n(\nu_2)$ are the corresponding frequencies and indices of refraction.⁶³ In the region above 2000 cm^{-1} the refractive index is practically frequency independent (see Fig. 7) and therefore $n(\nu_1) \approx n(\nu_2) = n$. Thus, for $\nu > 2000\text{ cm}^{-1}$, Eq. (5) reduces to $t = N/2n(\nu_1 - \nu_2)$ and is used to obtain directly the thickness of the film. The results are given in Table I, where comparison with the thickness data obtained with the fitting procedure shows a good agreement.

The measured transmittance T spectra shown in Figs. 5 and 6 were transformed into absorbance. A spectra ($A = -\log_{10} T$) to allow comparison with the data reported by Hudgens and Martin for thin films⁴⁸ and with those obtained in this study by analysis of the absorption coefficient spectra of bulk samples. The integrated intensities A_4 and A_3 were calculated by the procedure followed for bulk samples and the ratio A_4/A_3 is plotted in Fig. 3 versus AgI content. Although the present results show that A_4/A_3 follows the same trend versus AgI content in both thin films and bulk samples, the A_4/A_3 ratio of thin films is larger than that of the bulk samples. This finding is consistent also with the fact that the intensity of the 1320 cm^{-1} band relative to that at 965 cm^{-1} is larger for the calculated spectra, using $n(\nu)$ and $k(\nu)$ of

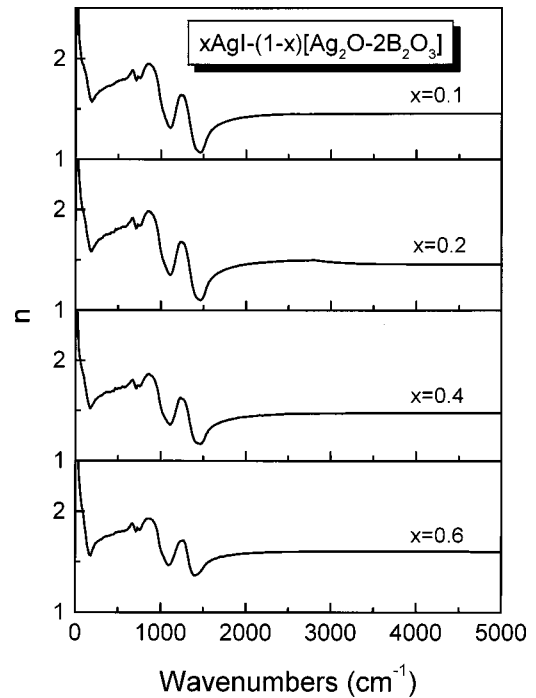


FIG. 7. Refractive index spectra of glasses in the system $x\text{AgI}-(1-x)[\text{Ag}_2\text{O}-2\text{B}_2\text{O}_3]$, obtained by Kramers-Kronig inversion of the reflectance spectra.

the bulk, than for the measured spectra of thin films (see Figs. 5 and 6). The origin of these findings and possible consequences will be discussed in a following section.

IV. DISCUSSION

A. Effect of AgI on the network structure of bulk glasses

Early NMR (Ref. 64) and more recent IR and Raman⁶⁰ studies of $y\text{Ag}_2\text{O}-(1-y)\text{B}_2\text{O}_3$ glasses have shown that for low Ag_2O contents ($y < 0.25$) the structural modification mechanism when Ag_2O is added to B_2O_3 involves mainly the transformation of neutral BO_3 triangles into charged borate tetrahedra BO_4^- . Therefore, the fraction of four-coordinated boron atoms, X_4 , obeys the law $X_4 = y/(1-y)$. For $y > 0.25$, X_4 deviates considerably from its theoretical value because of the formation of nonbridging oxygen (NBO) atoms in charged borate triangles, $\text{B}\text{O}_2\text{O}^-$. Thus the SRO of the borate network at the diborate composition ($y = 0.33$) can

TABLE I. Comparison of film thickness t data obtained by fitting Eq. (4) to the experimental transmittance spectra of $x\text{AgI}-(1-x)[\text{Ag}_2\text{O}-2\text{B}_2\text{O}_3]$ glasses and by applying Eq. (5), with $n(\nu_1) = n(\nu_2) = n$ being the value of the refractive index of the bulk glass for frequencies above 2000 cm^{-1} .

Mole fraction AgI (x)	t from Eq. (4) (μm)	t from Eq. (5) (μm)	n
0.1	2.46 ± 0.04	2.5 ± 0.1	1.44
0.2	3.35 ± 0.07	3.4 ± 0.1	1.44
0.2	5.19 ± 0.07	5.2 ± 0.1	1.44
0.4	4.53 ± 0.07	4.5 ± 0.1	1.48
0.6	3.02 ± 0.05	3.1 ± 0.1	1.60

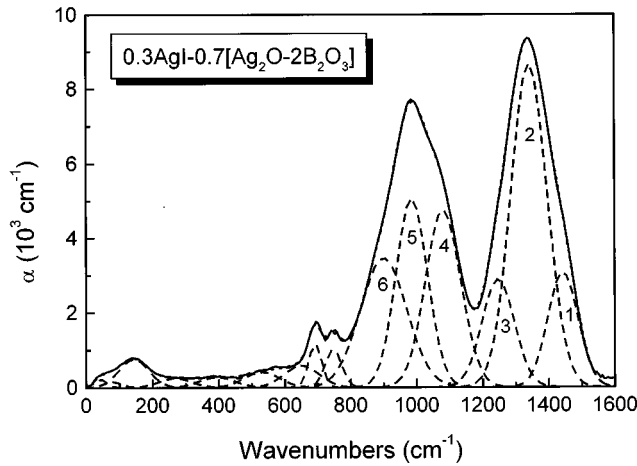


FIG. 8. Deconvolution of the absorption coefficient spectrum (solid line) of the 0.3AgI-0.7[Ag₂O-2B₂O₃] glass into Gaussian components (dashed lines). The simulated spectrum is shown by the dotted line.

be described in terms of borate triangles BØ₃ and BØ₂O⁻ and tetrahedra BØ₄⁻. These polyhedra participate in the formation of larger borate arrangements, with well-defined MRO, like the triborate and diborate groups.⁶⁵

Since addition of AgI to Ag₂O-2B₂O₃ glass is not expected to change the total formal negative charge on the borate network, the dependence of the A₄/A₃ ratio on AgI content (Fig. 3) can be understood in term of changes in the population of borate species. This can be expressed by the following chemical equilibrium⁶⁶ that takes place in the melt and involves the isomeric BØ₂O⁻ and BØ₄⁻ species



The data reported in Fig. 3 for bulk glasses indicate that when the AgI content is increased the above equilibrium shifts progressively to the left. For the quantification of this effect, it is necessary to evaluate the fractions X₄, X₃, and X₂ of BØ₄⁻, BØ₃, and BØ₂O⁻ species, respectively. Mass and charge balance considerations for the diborate composition give

$$X_2 + X_3 + X_4 = 1, \quad (7)$$

$$X_2 + X_4 = 0.5. \quad (8)$$

Thus X₃ = 0.5, i.e., the fraction of the BØ₃ units, is independent of the presence of AgI. To obtain X₂ and X₄, deconvolution of the absorption coefficient spectra was performed, as shown in Fig. 8 for a typical AgI-containing borate glass. It was found that the characteristic range of the stretching vibration modes of the borate network (800–1600 cm⁻¹) is best fitted with six Gaussian components; three of them are in the range of boron-oxygen triangles (1430–1450 cm⁻¹, 1325–1350 cm⁻¹, and 1220–1245 cm⁻¹), and the remaining bands in the range of borate tetrahedra (1070–1085 cm⁻¹, 980–995 cm⁻¹, and 890–905 cm⁻¹). The frequency of each band depends on composition, and it is determined with an accuracy of ±3 cm⁻¹. The corresponding error for the bandwidths is ±5 cm⁻¹ and the integrated intensities are accurate to ±3%.

Since two types of borate triangles (BØ₃ and BØ₂O⁻) contribute to the infrared activity in the ca 1200–1600 cm⁻¹ region, assignment of the three deconvoluted components in this region can be made. For the BØ₃ unit with D_{3h} point group symmetry, theory predicts the following normal modes of vibration: $\Gamma_{D_{3h}} = A_1'(R) = 2E'(IR, R) + A_2''(IR)$, with R and IR denoting Raman and infrared activity, respectively.⁶⁷ From these modes, the asymmetric stretching vibration of the borate triangle active in the infrared has E' symmetry. The six normal modes of vibration of the BØ₂O⁻ unit with C_{2v} symmetry are distributed as follows: $\Gamma_{C_{2v}} = 3A_1(IR, R) + B_1(IR, R) + 2B_2(IR, R)$, with two of these modes (A₁, B₂) corresponding to IR-active asymmetric stretching vibrations of the triangle. Thus replacement of a bridging by a nonbridging oxygen atom in BØ₃ triangles causes (a) the splitting of the doubly degenerate E' mode into two components of symmetry A₁ and B₂, and (b) the weak activation in the infrared of the symmetric stretching mode, A₁. Indeed, crystalline Li₂O-2B₂O₃ having a structure based on BØ₃ and BØ₄⁻ units in diborate arrangements presents a very strong infrared feature at ca 1390 cm⁻¹, while crystalline α-Li₂O-B₂O₃ consisting of BØ₂O⁻ units in metaborate chains exhibits two strong IR bands at ca 1445 and 1260 cm⁻¹ and a shoulder at ca 1510 cm⁻¹.⁵⁹ On these grounds, it is reasonable to attribute the 1325–1350 cm⁻¹ band to the asymmetric stretching vibration of BØ₃ units (band 2 in Fig. 8), and the two remaining bands at 1220–1245 cm⁻¹ and 1430–1450 cm⁻¹ (bands 3 and 1 in Fig. 8) to the asymmetric stretching vibration of BØ₂O⁻ units with C_{2v} symmetry. It is noted that detailed assignments of the bands in the range of boron-oxygen tetrahedra (800–1200 cm⁻¹, bands 4, 5, and 6 in Fig. 8) is not essential for the analysis presented below.

Denoting by A_i the integrated intensity of the ith component band (1 ≤ i ≤ 6) normalized by the total integrated intensity of the stretching modes (800–1600 cm⁻¹ range) and following the assignments made above, the fractions X₂ and X₄ are given by

$$X_2 = A_1/\alpha_1, \quad X_2 = A_3/\alpha_3, \quad X_4 = (A_4 + A_5 + A_6)/\alpha_4, \quad (9)$$

where α₁ and α₃ are the normalized absorption coefficients of the corresponding modes (A₁, B₂) of BØ₂O⁻ units and α₄ is a normalized average absorption coefficient of BØ₄⁻ tetrahedra. From Eqs. (8) and (9) it is obvious that there are five unknown parameters (X₂, X₄, α₁, α₃, and α₄) and four equations. This difficulty can be handled if the absorption coefficients α_i of borate species are assumed to exhibit negligible dependence on the AgI content. Then, by combining Eqs. (9) for two glasses k and l, we obtain the following ratios:

$$\frac{A_{1k}}{A_{1l}} = \frac{A_{3k}}{A_{3l}} = \frac{X_{2k}}{X_{2l}} = F_{2kl}, \quad (10)$$

$$\frac{(A_4 + A_5 + A_6)_k}{(A_4 + A_5 + A_6)_l} = \frac{X_{4k}}{X_{4l}} = F_{4kl}. \quad (11)$$

The fractions X_{2k}, X_{2l}, X_{4k}, and X_{4l} for glasses k and l can be obtained now by solving the system of Eqs. (10), (11),

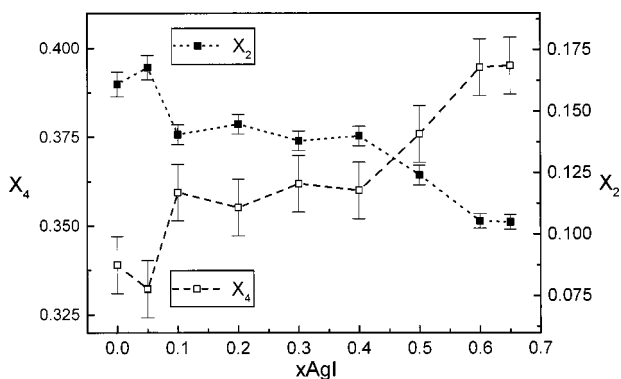


FIG. 9. Fractions X_4 and X_2 of borate tetrahedra ($B\text{Ø}_4^-$) and triangles ($B\text{Ø}_2\text{O}^-$), respectively, as a function of AgI content in $x\text{AgI}-(1-x)[\text{Ag}_2\text{O}-2\text{B}_2\text{O}_3]$ glasses.

and (8) and noting that there is one Eq. (8) for each glass k and l . The results, averaged over all possible combinations of spectra, are reported in Fig. 9 versus AgI content. The fraction of four-coordinated boron atoms, X_4 , obtained in this study varies from 0.34 ($x=0$) to 0.39 ($x=0.65$) with an experimental error estimated to be about 2.5%, while the fraction X_2 varies from 0.16 to 0.11 with the experimental error being about 3%. The changes of X_4 and X_2 resulting from the AgI addition are well outside our experimental error in determining these fractions. It is noted also that the $X_4 = 0.34$ value for the $\text{Ag}_2\text{O}-2\text{B}_2\text{O}_3$ glass found by the IR analysis is in very good agreement with the NMR result ($N_4=0.35$) reported by Kim and Bray.⁶⁴

The data in Fig. 9 demonstrate the notion that accommodation of AgI by the diborate glass network is effected by local rearrangements of the SRO structure, as manifested by the progressive shift of equilibrium (6) to the left. Once the fractions X_4 and X_2 are obtained, a quasiequilibrium constant K_{eq} for reaction (6) can be evaluated by

$$K_{\text{eq}} = \frac{X_2}{X_4}, \quad (12)$$

where activity coefficients are ignored. As shown in Fig. 10(a), K_{eq} decreases systematically as the AgI content increases. The equilibrium constant of a reaction depends on both pressure and temperature, but the present glasses were prepared under identical quenching conditions. Therefore, K_{eq} refers mostly to the fictive temperature at which the structure of the supercooled liquid was “frozen” into the glassy state. Since fictive temperatures for these glasses are not available, we employ the glass transition temperatures T_g determined by Chiodelli *et al.*⁴² and observe that T_g shows the same dependence on AgI content as the equilibrium constant [see Fig. 10(b)]. Thus it appears that the decrease of T_g is directly related to the decrease of K_{eq} caused by the AgI addition. These findings are consistent with the results of the statistical mechanical calculations of Araujo⁶⁸ for the correlation of temperature and borate speciation in alkali borate glasses. In particular, Araujo finds that X_4 is a function of both temperature and composition, and that for the diborate composition X_4 increases with decreasing temperature.

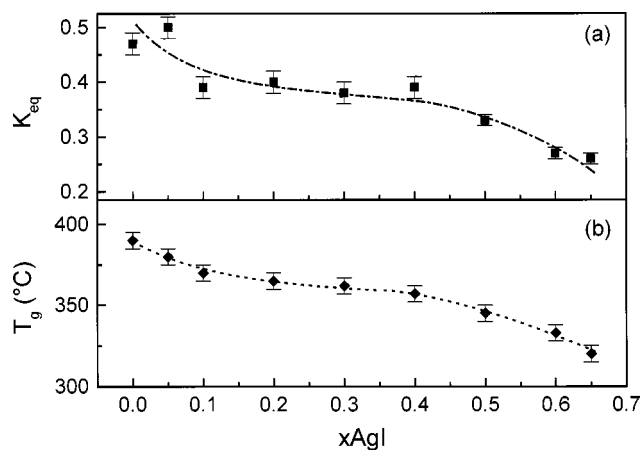


FIG. 10. Effect of AgI on the equilibrium constant of reaction (6), $K_{\text{eq}} = X_2/X_4$ (a) and on the glass transition temperature T_g (b) for glasses $x\text{AgI}-(1-x)[\text{Ag}_2\text{O}-2\text{B}_2\text{O}_3]$. T_g data are those reported by Chiodelli *et al.* (Ref. 42). Lines are drawn as guides to the eye.

From the dependence of K_{eq} on T_g we can estimate the enthalpy change (ΔH) associated with reaction (6) according to

$$\ln K_{\text{eq}} = -\frac{\Delta H}{RT_g} + \frac{\Delta S}{R}, \quad (13)$$

where ΔS is the entropy change and R is the gas constant. From the least-squares fitting of the $\ln K_{\text{eq}}$ vs $1/T_g$ plot in Fig. 11, it is found that $\Delta H = 32 \pm 5$ kJ/mol and $\Delta S = 42 \pm 5$ J/Kmol of boron. The value of ΔH is consistent with that reported recently by Sen *et al.* (35 ± 12 kJ/mol of boron) for the reaction $B\text{Ø}_4^- \rightleftharpoons B\text{Ø}_3 + \text{NBO}$ in sodium borate melts.⁶⁹

It is clear from the above discussion that accommodation of a relatively inert metal halide salt, such as AgI, in a modified binary glass matrix affects the SRO structure. These changes in SRO are responsible for the decrease of T_g and presumably the decrease of the fictive temperature at which the structure of the supercooled liquid is arrested into the glassy state. For the diborate system, the changes in SRO are effected by the transformation of $B\text{Ø}_2\text{O}^-$ triangles into $B\text{Ø}_4^-$

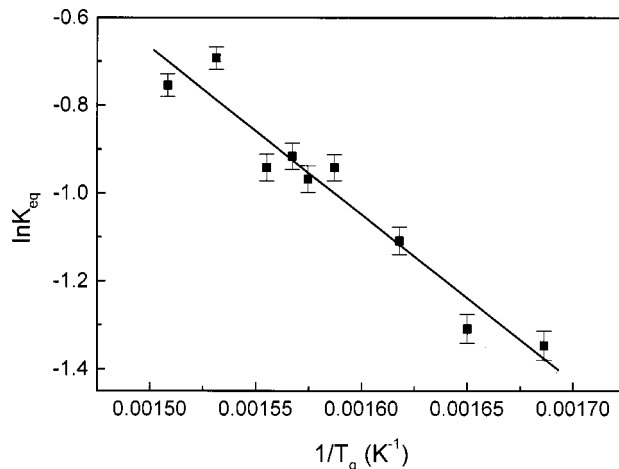


FIG. 11. Dependence of the equilibrium constant K_{eq} of reaction (6) on the glass transition temperature T_g . The solid line is the least-squares fitting of the data.

tetrahedra. This mechanism favors a better packing of the borate backbone, because the effective volume of borate tetrahedra is approximately 70% smaller than that of their isomeric triangles,⁷⁰ and thus this process would leave more room to be occupied by the bulky AgI. This is also consistent with the results of x-ray and neutron diffraction studies in this system that indicate an improvement of the medium-range order of the glass by addition of AgI.⁵¹⁻⁵³

For reasons explained in Sec. III A, the above detailed analysis for the diborate family can not be performed for glasses in the pyroborate series. Therefore, the spectroscopic data will be discussed only in a qualitative manner. Figure 4 shows the presence of intense bands at 955 and 1030 cm^{-1} due to BO_4^- tetrahedra, despite the fact that in glasses of the pyroborate composition (67 mol% of metal oxide) the fraction of BO_4^- is almost zero.⁵⁹ This situation can be understood in terms of the following equilibrium:⁶⁶



which appears to be favored by AgI. In view of this it is of interest to note that crystalline silver-orthoborate (Ag_3BO_3) and metaborate (AgBO_2) have been prepared under oxygen pressure, but the pyroborate crystal ($\text{Ag}_4\text{B}_2\text{O}_5$) has not been prepared so far.^{71,72} Therefore, the stabilization of pyroborate ($\text{B}_2\text{O}_5^{4-}$) species in the present silver-borate glasses seems to result from the disproportionation reaction [Eq. (14)] that leads to the coexistence of orthoborate (BO_3^{3-}) and metaborate (BO_4^-) species in the presence of AgI.

B. Spectra of thin films and comparison with bulk samples

The data reported in Fig. 3 show that (a) thin films exhibit larger A_4/A_3 values than bulk samples, (b) A_4/A_3 decreases upon increasing film thickness, and (c) the values reported by Hudgens and Martin⁴⁸ for thin films are larger than those obtained in this work. To evaluate these findings we consider first the effect of film thickness on the A_4/A_3 value. For this purpose, transmittance and absorbance spectra were calculated using Eq. (4) and the $n(\nu)$ and $k(\nu)$ spectra of bulk samples. Typical calculated spectra are shown in Fig. 12 for films having the same composition, $0.2\text{AgI}-0.8[\text{Ag}_2\text{O}-2\text{B}_2\text{O}_3]$, but different thickness. As shown in Fig. 12(b), the intensity of the 970 cm^{-1} band (borate tetrahedra) appears to decrease relative to that at 1325 cm^{-1} (borate triangles) as the thickness of the film increases. Obviously, this is not due to real structural differences because all spectra were computed on the basis of the same set of $n(\nu)$ and $k(\nu)$. Instead, the spectra of thin films represent the interference between the corresponding spectrum at the first interface of the sample and the multiple internal reflections between the two interfaces. Therefore, each spectrum results from the combined contribution of the real spectrum of the sample and a harmonic oscillatory interference term.

The degree of change of the relative intensity of the 970 and 1325 cm^{-1} bands depends on the period ($1/2nt$) and the amplitude of interference [$R^N D^N$, where R and D are given by Eqs. (4b) and (4c) and N is the order of interference]. Both the period and amplitude of interference decrease upon increasing film thickness, and this is demonstrated also in Fig. 12 for the calculated spectra. The calculated dependence of A_4/A_3 on film thickness is shown in Fig. 13 for the com-

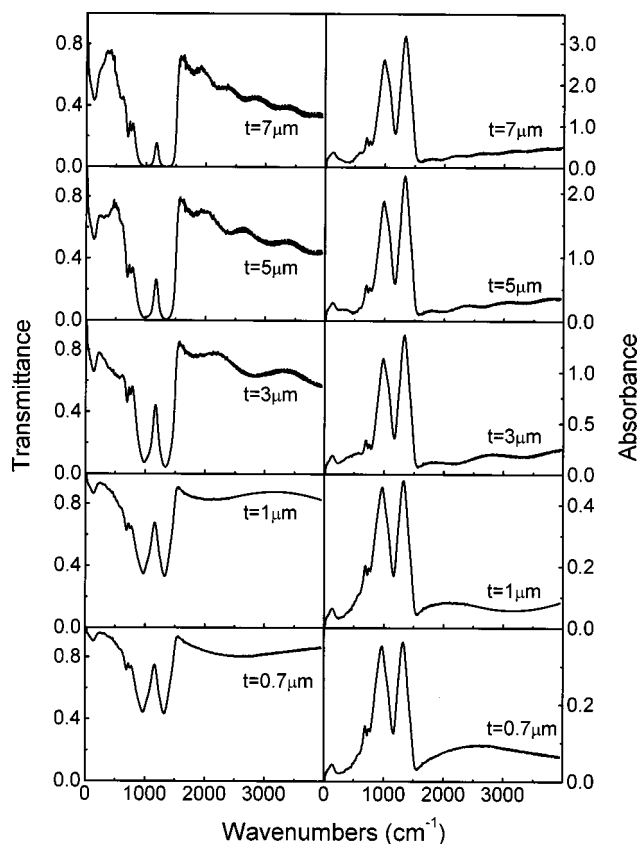


FIG. 12. Calculated transmittance and absorbance spectra using Eq. (4) and the optical constants [$n(\nu)$ and $k(\nu)$] obtained by Kramers-Kronig analysis of the specular reflectance spectrum of the bulk glass $0.2\text{AgI}-0.8[\text{Ag}_2\text{O}-2\text{B}_2\text{O}_3]$.

position $0.2\text{AgI}-0.8[\text{Ag}_2\text{O}-2\text{B}_2\text{O}_3]$ and shows that in the range $t_1 < t < t_2$ the value of A_4/A_3 changes rapidly with film thickness. We have repeated the same calculations for all compositions of interest and found that both threshold thickness values t_1 and t_2 increase almost linearly with AgI content of the glass, as shown in the inset of Fig. 13. This trend

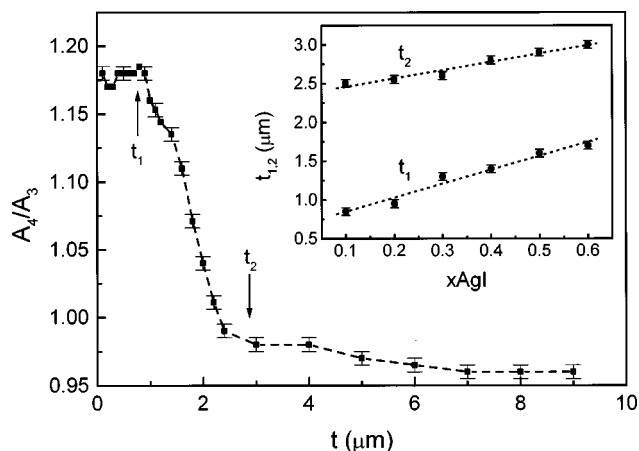


FIG. 13. Dependence of the relative integrated absorption A_4/A_3 on film thickness t for glassy films with composition $0.2\text{AgI}-0.8[\text{Ag}_2\text{O}-2\text{B}_2\text{O}_3]$. For $t_1 < t < t_2$ the ratio A_4/A_3 shows a strong dependence on film thickness. The inset illustrates the dependence of t_1 and t_2 on AgI content for glasses in the system $x\text{AgI}-(1-x)[\text{Ag}_2\text{O}-2\text{B}_2\text{O}_3]$.

can be attributed to the progressive decrease of the number of borate species per unit thickness of the film with AgI addition.

The points presented above explain our experimental evidence that A_4/A_3 decreases when the film becomes thicker and approaches the value obtained from the absorption coefficient spectrum of the bulk sample. In practice, though, transmittance values below ca 0.5–1% cannot be measured with accuracy even with modern spectrometers. With reference to Fig. 12 this indicates that the 970 and 1325 cm^{-1} bands in the experimental spectrum would exhibit saturation effects when the film thickness exceeds $\approx 6 \mu\text{m}$, and thus any variations of A_4/A_3 with composition would be very difficult to distinguish.

Regarding the comparison of A_4/A_3 values found for thin films with those obtained from the absorption coefficient spectra of bulk samples,⁴⁸ it is noted that they cannot be the same, even when thick films are considered. Indeed, for thick films, Eq. (4) can be reduced to

$$T = |1 - r_c^2|^2 e^{-\alpha t}. \quad (15)$$

Therefore, the ratio A_4/A_3 calculated from the absorbance spectrum $A(\nu)$ will be

$$\frac{A_4}{A_3} = \frac{\int_{\text{tetrahedra}} A(\nu) d\nu}{\int_{\text{triangles}} A(\nu) d\nu} = \frac{t \int_{\text{tetrahedra}} \alpha(\nu) d\nu - \int_{\text{tetrahedra}} \ln|1 - r_c^2|^2 d\nu}{t \int_{\text{triangles}} \alpha(\nu) d\nu - \int_{\text{triangles}} \ln|1 - r_c^2|^2 d\nu}, \quad (16)$$

and the corresponding ratio A_4/A_3 calculated from the absorption coefficient spectrum $\alpha(\nu)$ of the bulk glass is

$$\frac{A_4}{A_3} = \frac{\int_{\text{tetrahedra}} \alpha(\nu) d\nu}{\int_{\text{triangles}} \alpha(\nu) d\nu}. \quad (17)$$

It is evident from Eqs. (16) and (17) that the value of A_4/A_3 obtained through the $A(\nu)$ spectrum is different to that calculated from the $\alpha(\nu)$ spectrum. Thus a quantitative comparison between the results of the two methods cannot be made. It is noted also that the absorbance spectra reported by Hudgens and Martin were measured on films with thickness ~ 10 – $100 \mu\text{m}$, as indicated by these authors.⁴⁸ Our findings in Fig. 12 indicate that, even for the thinnest films ($\sim 10 \mu\text{m}$), the spectra should exhibit saturation effects in the region of strong absorption (800 – 1500cm^{-1}).

An additional difficulty in comparing the spectra of thin films and bulk samples arises from the possibility that these can exhibit structural differences because of their different thermal histories. As described in the experimental section, bulk samples were obtained by splat quenching the melt immediately after removal from the furnace, while for thin films the melt was allowed to cool first slowly, for viscosity to reach an appropriate value, and then very quickly by film blowing. Under such conditions, it is reasonable to assume that bulk samples have higher fictive temperatures, and according to Eq. (4), the fraction of borate tetrahedra would be larger in thin films than in bulk samples. Therefore, besides the optical effects discussed above, there are structural reasons for thin films and bulk samples to exhibit different values of the A_4/A_3 ratio.

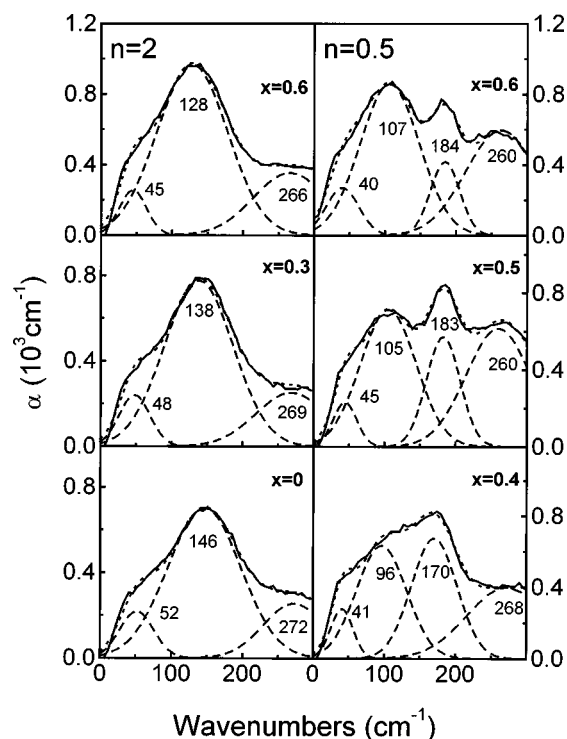


FIG. 14. Far-infrared spectra (solid lines) of glasses $x\text{AgI}-(1-x)[\text{Ag}_2\text{O}-n\text{B}_2\text{O}_3]$ with $n=2$, $0 \leq x \leq 0.6$ (diborate) and $n=0.5$, $0.4 \leq x \leq 0.6$ (pyroborate), deconvoluted into Gaussian component bands (dashed lines). The simulated spectra are shown by dotted lines.

C. Far-IR spectra and the nature of silver ion sites in AgI-containing glasses

In this section we focus on the IR profiles below ca 300cm^{-1} where the vibrations of metal ions in their sites are active, and thus useful information regarding the nature of anionic sites hosting silver ions can be extracted from spectral analysis. Characteristic far-infrared absorption spectra are shown in expanded frequency and intensity scales in Fig. 14(a) and 14(b) for glasses in the diborate and pyroborate families, respectively.

Starting with the diborate family, because it includes the AgI-free composition, we note that the spectra of the AgI-containing glasses show no remarkable differences compared to that of the $\text{Ag}_2\text{O}-2\text{B}_2\text{O}_3$ glass. Nevertheless, it is observed that the main peak at ca 145cm^{-1} ($x=0$) shifts progressively to lower frequency as x increases. Because of their highly asymmetric nature, the far-IR profiles were deconvoluted using the minimum number of component bands that give a reasonable agreement between experimental and calculated spectrum.^{55–57} The spectrum of the $x=0$ glass has been fitted with three Gaussian components centered at 52cm^{-1} (ν_L), 146cm^{-1} (ν_H), and 272cm^{-1} . The last component can be attributed to a borate network deformation mode, while the bands with frequencies designated by ν_L and ν_H can be assigned to Ag-O vibrations, most probably in two anionic site environments involving oxygen atoms of the borate network.⁶⁰ This proposition is compatible with earlier EXAFS results for the same glass ($x=0$) that indicate the presence of two coordination environments for silver ions differing in coordination number and Ag-O distance.⁷³

The ability of silver ions to adopt different coordination environments depending on the charge density of oxygen atoms is demonstrated very well in crystalline Ag-borate compounds. For example, in $\text{Ag}_2\text{O}\cdot 4\text{B}_2\text{O}_3$ all oxygen atoms bridge two boron centers and silver ions fulfill their bonding requirements in sevenfold and eightfold coordinated sites.⁷⁴ The orthoborate crystal $\text{Ag}_2\text{O}\cdot 0.33\text{B}_2\text{O}_3$, where all oxygen atoms are nonbridging and the silver requirements are met with twofold coordination to oxygen,⁷² provides the other extreme. In crystalline silver-metaborate, $\text{Ag}_2\text{O}\cdot \text{B}_2\text{O}_3$, there are both bridging oxygen atoms in interlinked BO_4^- tetrahedra and $\text{B}\text{O}_2\text{O}^-$ triangles and nonbridging oxygen atoms in $\text{B}\text{O}_2\text{O}^-$ triangles. This situation allows silver ions to explore a range of sites with coordination numbers varying from 3 to 6.⁷¹ As discussed elsewhere,⁷⁵ small metal-oxygen distance and high charge density characterize sites with small coordination numbers, both factors leading to a high metal-oxygen stretching frequency.⁷⁵ On these grounds, it is reasonable to attribute the higher-frequency band (146 cm^{-1}) of the $x=0$ diborate glass to Ag-O vibrations in a distribution of oxide sites with relatively low coordination numbers (H sites). Similarly, the lower-frequency component (52 cm^{-1}) can be attributed to Ag-O vibrations in a distribution of sites with larger coordination numbers (L sites)

The spectra of the AgI-containing diborate glasses could be fitted also with three Gaussian components as shown in Fig. 14(a). Following the assignments for the $x=0$ glass, the bands at $50\text{--}45\text{ cm}^{-1}$ (ν_L) and $146\text{--}128\text{ cm}^{-1}$ (ν_H) are attributed to localized vibrations of Ag ions in their suitable sites and the one at ca 270 cm^{-1} to a network mode. The nature of sites hosting silver ions in these glasses will be discussed after considering the spectra of pyroborate glasses.

Deconvolution of the far-IR profiles of pyroborate glasses [Fig. 14(b)] showed the presence of at least four components, i.e., at ca 40 , 175 , and 260 cm^{-1} and the fourth component at ca 100 cm^{-1} . By analogy with the binary $\text{Ag}_2\text{O}\cdot 2\text{B}_2\text{O}_3$ glass, the components at ca 40 and 175 cm^{-1} are attributed to Ag-O vibrations in sites made primarily by oxygen atoms of the borate network, sites L and H , respectively, and the 260 cm^{-1} feature is attributed to a network mode. As shown in the spectra, both the frequency and intensity of the ca 100 cm^{-1} band increase with AgI content. In view of these findings and our previous work,^{46,47} we assign this band to localized vibrations of Ag^+ ions in primarily iodide environments. This assignment is consistent also with the fact that crystalline $\beta\text{-AgI}$ (wurtzite) and $\alpha\text{-AgI}$ (superionic phase) exhibit their main infrared absorption at $\sim 110\text{ cm}^{-1}$, due to the Ag-I stretching mode $\nu_{\text{Ag-I}}$, in a tetrahedral iodide environment.^{76,77} The increase of $\nu_{\text{Ag-I}}$ from 96 to 107 cm^{-1} as the AgI content increases from $x=0.4$ to 0.6 could indicate a gradual aggregation of silver-iodide sites into clusters, the size of which cannot be estimated at present from the infrared spectroscopic data. It is noted that the spectroscopic data suggest also a slight variation of the nature of H sites with addition of AgI and, in particular, a gradual strengthening of the Ag-O interactions since ν_H increases with x [Fig. 14(b)]. This effect can be understood in terms of chemical equilibrium (14) that was found to shift towards the orthoborate triangles (BO_3^{3-}) in the presence of AgI. The oxygen atoms of such borate species participate in the formation of sites with high charge density and small coordination

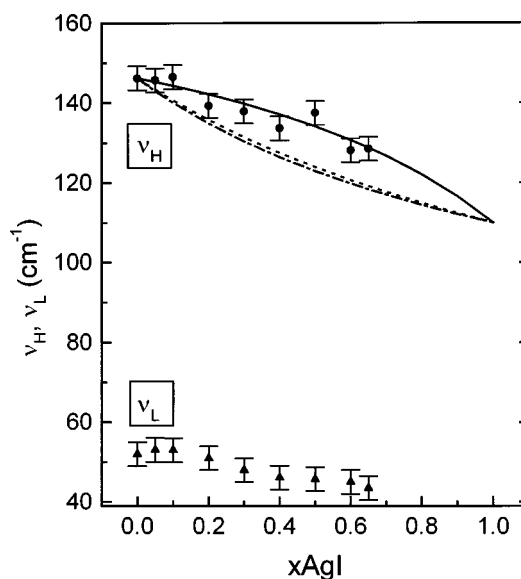


FIG. 15. Effect of AgI addition on the Ag^+ ion motion frequencies (ν_H, ν_L) in $x\text{AgI}\cdot(1-x)[\text{Ag}_2\text{O}\cdot 2\text{B}_2\text{O}_3]$ glasses. The solid line was calculated by Eq. (18). Dash-dotted and dotted lines were calculated by Eq. (19) using the dipole and tetrahedral site approximations, respectively. For details see text.

numbers,⁷² and this would naturally lead to higher Ag-O stretching frequencies. Therefore, the analysis of the far-IR profiles of AgI-doped pyroborate glasses suggests that silver ions are distributed in a range of environments. A fraction of silver ions occupy oxide network sites (L and H sites) and the rest of them are present in iodide sites with varying degree of organization.

Based on the above analysis, we can now seek a more detailed description of the nature of silver ion sites in AgI-doped diborate glasses. As shown in Fig. 15, both ν_H and ν_L decrease with increasing AgI content, this trend being more pronounced for ν_H . One way of explaining this result is by assuming that the H band in AgI-doped diborate glasses is the convolution of two close-lying components; one at ca 146 cm^{-1} (oxide band) and another at ca 110 cm^{-1} (iodide band). As the AgI content increases, the former component is reduced in intensity, while the latter exhibits the opposite effect. On the overall, the convoluted H band appears to shift to lower frequency with addition of AgI. According to this simple model, which ignores interactions between neighboring oxide and iodide sites, the frequency ν_H of the convoluted band can be approximated by

$$\nu_H = f_I \nu_{\text{Ag-I}} + f_O \nu_{\text{Ag-O}}, \quad (18)$$

where $\nu_{\text{Ag-I}} = 110\text{ cm}^{-1}$, $\nu_{\text{Ag-O}} = 146\text{ cm}^{-1}$, and f_I and f_O are the fractions of silver ions in iodide and H -type oxide sites, respectively. Since the intensity of the L band in the $x=0$ glass spectrum contributes less than $\sim 10\%$ to the total Ag-ion motion activity, we assume for simplicity that all Ag ions introduced by Ag_2O contribute to the H oxide band. Hence the fractions in Eq. (18) are given by $f_I = x/(2-x)$ and $f_O = 2(1-x)/(2-x)$. Calculated ν_H frequencies by employing Eq. (18) are shown by the solid line in Fig. 15.

A different model to explore the trend of ν_H with x could involve the progressive substitution of oxygen atoms by io-

dide ions in the coordination sphere of silver, i.e., the formation of mixed oxyiodide sites. This process will affect the reduced mass and force constant and thus the frequency of the silver-site vibration. Denoting by k_{eff} and μ_{eff} the effective force constant and reduced mass of the silver-oxyiodide site vibration, ν_H would be simply

$$\nu_H = \frac{1}{2\pi c} \sqrt{\frac{k_{\text{eff}}}{\mu_{\text{eff}}}}, \quad (19)$$

where c is the speed of light, and k_{eff} and μ_{eff} are approximated by

$$k_{\text{eff}} = f_I k_{\text{Ag-I}} + f_O k_{\text{Ag-O}}, \quad (20a)$$

$$\mu_{\text{eff}} = f_I \mu_{\text{Ag-I}} + f_O \mu_{\text{Ag-O}}, \quad (20b)$$

where $k_{\text{Ag-I}}$ and $\mu_{\text{Ag-I}}$ are the force constant and reduced mass of silver-site vibration in crystalline AgI, and $k_{\text{Ag-O}}$ and $\mu_{\text{Ag-O}}$ are the corresponding quantities for silver oxide sites in $\text{Ag}_2\text{O} \cdot 2\text{B}_2\text{O}_3$ glass. The reduced masses $\mu_{\text{Ag-I}}$ and $\mu_{\text{Ag-O}}$ were calculated using the dipole and the tetrahedral-site approximation,⁷⁸ and the corresponding force constants $k_{\text{Ag-I}}$ and $k_{\text{Ag-O}}$ were calculated subsequently from the expression $k = 4\pi^2 c^2 \nu^2 \mu$, where the frequencies are $\nu_{\text{Ag-I}} = 110 \text{ cm}^{-1}$ and $\nu_{\text{Ag-O}} = 146 \text{ cm}^{-1}$. Calculated ν_H frequencies on the basis of the silver-oxyiodide model [Eqs. (19) and (20)] are shown also in Fig. 15 for the dipole (dash-dotted line) and tetrahedral (dotted line) approximations.

Comparison in Fig. 15 of the experimental ν_H data with the results of the two simple models considered above indicates that a model in between these two extreme cases, i.e., the existence of a range of oxide, iodide, and mixed oxyiodide environments for silver ions, is more realistic for diborate glasses. However, the far-infrared results of pyroborate glasses suggest that silver ions occupy mainly oxide and iodide sites. Upon increasing the AgI content the iodide sites grow probably in size as monitored by the progressive increase of $\nu(\text{Ag-I})$. Overall, the formation and nature of silver-iodide sites in $x\text{AgI} \cdot (1-x)[\text{Ag}_2\text{O} \cdot n\text{B}_2\text{O}_3]$ glasses were found to depend on both the $\text{Ag}_2\text{O}/\text{B}_2\text{O}_3$ ratio and the AgI content.

V. CONCLUSIONS

AgI-containing superionic glasses



with $n=2$ (diborate) and $n=0.5$ (pyroborate), have been prepared and studied by infrared spectroscopy. The purpose of this work is to investigate the structure of the glass network and its dependence on the AgI doping salt, as well as the nature of sites occupied by the charge carrying silver ions. Glasses were obtained in bulk and thin film forms using AgNO_3 as the source of Ag_2O , and their spectra were measured by the specular reflectance and transmission techniques, respectively. Reflectance spectra were analyzed by the Kramers-Kronig inversion and transmission spectra were simulated by taking into account the multiple reflections inside the film.

The analysis of the midinfrared profiles of diborate bulk compositions showed that the short-range order of the glass

network consists of borate triangles ($\text{B}\text{O}_2\text{O}^-$ and BO_3) and tetrahedra (BO_4^-). Spectral deconvolution was performed to quantify the glass structure by calculating the mole fractions of the local borate structural units. It was found that the fractions of $\text{B}\text{O}_2\text{O}^-$ triangles and BO_4^- tetrahedra depend on the AgI content of the glass, and this effect was explained in terms of the isomerization reaction $\text{B}\text{O}_4^- \rightleftharpoons \text{B}\text{O}_2\text{O}^-$ between metaborate tetrahedra and triangles. A quasiequilibrium constant K_{eq} of this reaction was calculated from the spectroscopic data and found to decrease with increasing AgI content of the glass. It was concluded that the AgI-induced transformation of $\text{B}\text{O}_2\text{O}^-$ triangles into BO_4^- tetrahedra leads to a better packing of the borate backbone and thus to an improvement of the medium-range order of the glass.

Similarly, it was shown that the network structure of pyroborate glasses can be understood on the basis of the disproportionation of pyroborate dimers ($\text{B}_2\text{O}_5^{4-}$) to orthoborate monomers (BO_3^{3-}) and metaborate tetrahedra, i.e., $\text{B}_2\text{O}_5^{4-} \rightleftharpoons \text{BO}_3^{3-} + \text{B}\text{O}_4^-$. The spectroscopic data indicate that AgI favors this disproportionation reaction and thus explain glass formation in the silver-pyroborate system, despite the fact that the $\text{Ag}_2\text{O} \cdot 0.5\text{B}_2\text{O}_3$ composition does not vitrify or form a crystalline phase.

The study of the infrared transmission spectra of thin films in the diborate family showed that the relative intensity of the absorption envelope due the borate tetrahedra decreases with increasing film thickness and approaches the behavior of the corresponding bulk glass. It was demonstrated that the main origin of this trend is traced to optical effects and, in particular, to the strong dependence of the period and amplitude of the background interference wave on film thickness. Besides optical effects, thin films and bulk glassy samples may exhibit differences in thermal history that can lead to structural variations and thus to additional spectral differences. Therefore, direct (quantitative) comparison of infrared spectral data of thin films and bulk glasses should be avoided, since it may lead easily to erroneous conclusions.

The far-infrared absorption spectra of AgI-doped pyroborate glasses showed that, besides the presence of the two bands at ca 40 and 175 cm^{-1} arising from the vibration of silver ions in oxide sites, a third band develops at ca 100 cm^{-1} as AgI is added to the glass. This new feature was assigned to the localized vibration of silver ions in primarily iodide sites. The intensity and resonance frequency of this band were found to increase with AgI content, suggesting the organization of silver-iodide units into tetrahedral sites such as those found in crystalline AgI. The aggregation of silver-iodide sites into AgI-like pseudophases cannot be excluded, though the dimensions of such domains cannot be estimated by infrared.

In contrast to pyroborates, the far-infrared profiles of diborate glasses could be simulated with only two silver-ion motion bands. The resonance frequency of the stronger component was found to decrease from 146 to 128 cm^{-1} as the AgI content increases from $x=0$ to 0.65. The experimental data were compared with the results of two simple-extreme models. The first considers the formation of separate silver-oxide and silver-iodide sites with varying population, and the second proposes the formation of only mixed oxy-iodide environments. Comparison with the experimental results shows

that the existence of a range of sites for silver ions including oxide, iodide, and mixed I/O environments describes better the AgI-containing diborate glasses. Therefore, it is concluded that the extent of formation and organization of separate AgI-like sites in $x\text{AgI}-(1-x)[\text{Ag}_2\text{O}-n\text{B}_2\text{O}_3]$ glasses is a function of both Ag_2O and AgI content.

ACKNOWLEDGMENTS

This work was supported by the Greek General Secretariat for Research and Technology (PENED Program No. 1065/95). We thank Dr. J. A. Kapoutsis for his help with spectral measurements and for many helpful discussions.

- *Author to whom correspondence should be addressed. FAX: 30-1 7273794. Electronic address: eikam@eie.gr
- ¹ *Fast Ion Transport in Solids*, edited by P. Vashista, J. N. Mundy, and G. K. Shenoy (Elsevier, New York, 1979).
 - ² T. Minami, *J. Non-Cryst. Solids* **73**, 273 (1985).
 - ³ H. L. Tuller and M. W. Basroum, *J. Non-Cryst. Solids* **73**, 331 (1985).
 - ⁴ H. L. Tuller, D. P. Button, and D. R. Uhlmann, *J. Non-Cryst. Solids* **40**, 93 (1980).
 - ⁵ D. Ravaine, *J. Non-Cryst. Solids* **73**, 287 (1985).
 - ⁶ M. D. Ingram, *Phys. Chem. Glasses* **28**, 215 (1985).
 - ⁷ J. L. Souquet, *Solid State Ionics* **28-30**, 693 (1988).
 - ⁸ C. A. Angell, *Annu. Rev. Phys. Chem.* **43**, 693 (1992).
 - ⁹ C. C. Hunter and M. D. Ingram, *Solid State Ionics* **14**, 31 (1984).
 - ¹⁰ S. W. Martin, *Solid State Ionics* **18-19**, 472 (1986).
 - ¹¹ A. Magistris, G. Chiodelli, and A. Schiraldi, *Electrochim. Acta* **23**, 585 (1978).
 - ¹² A. Magistris, G. Chiodelli, and A. Schiraldi, *Electrochim. Acta* **24**, 203 (1979).
 - ¹³ T. Minami, K. Imazawa, and T. Tanaka, *J. Non-Cryst. Solids* **42**, 469 (1980).
 - ¹⁴ T. Minami, Y. Ikeda, and T. Tanaka, *J. Non-Cryst. Solids* **52**, 159 (1982).
 - ¹⁵ T. Minami, T. Shimizu, and T. Tanaka, *Solid State Ionics* **9-10**, 577 (1983).
 - ¹⁶ T. Minami, M. Tatsumisago, and N. Machida, in *Glass Science and Technology*, edited by G. D. Chryssikos and E. I. Kamitsos, *Chimica Chronica, New Series* (Assoc. of Greek Chemists, Athens, 1994), Vol. 23, p. 227.
 - ¹⁷ Y. Kowada, H. Adachi, M. Tatsumisago, and T. Minami, *J. Non-Cryst. Solids* **232-234**, 497 (1998).
 - ¹⁸ B. Carette, M. Ribes, and J. L. Souquet, *Solid State Ionics* **9-10**, 735 (1983).
 - ¹⁹ M. Tatsumisago, T. Minami, and M. Tanaka, *Glastech. Ber.* **56K**, 845 (1983).
 - ²⁰ A. Levasseur, R. Olazcuaga, M. Kballa, M. Zahir, and P. Haggemuller, *C. R. Acad. Sci.* **293**, 563 (1981).
 - ²¹ B. Barrau, M. Ribes, M. Maurin, A. Kone, and J. L. Souquet, *J. Non-Cryst. Solids* **37**, 1 (1980).
 - ²² C. A. Angell, *Solid State Ionics* **18-19**, 72 (1986).
 - ²³ J. Kincs and S. W. Martin, *Phys. Rev. Lett.* **76**, 70 (1996).
 - ²⁴ O. L. Anderson and D. A. Stuart, *J. Am. Ceram. Soc.* **37**, 573 (1954).
 - ²⁵ D. Ravaine and J. L. Souquet, *Phys. Chem. Glasses* **18**, 27 (1977).
 - ²⁶ D. Ravaine and J. L. Souquet, *Phys. Chem. Glasses* **19**, 115 (1978).
 - ²⁷ G. N. Greaves, *J. Non-Cryst. Solids* **71**, 203 (1985).
 - ²⁸ K. Funke, *Prog. Solid State Chem.* **22**, 11 (1993).
 - ²⁹ A. Bunde, M. D. Ingram, P. Maass, and K. L. Ngai, *J. Non-Cryst. Solids* **131-133**, 1109 (1991).
 - ³⁰ A. Bunde, M. D. Ingram, and P. Maass, *J. Non-Cryst. Solids* **172-174**, 1222 (1994).
 - ³¹ M. Tachez, R. Mercier, J. P. Malugani, and A. T. Dianoux, *Solid State Ionics* **20**, 93 (1980).
 - ³² G. Carini, M. Cutroni, M. Frederico, G. Galli, and G. Tripodo, *Phys. Rev. B* **30**, 7212 (1984).
 - ³³ A. Schiraldi, E. Pezzari, and P. Baldini, *J. Phys. Chem.* **89**, 1528 (1985).
 - ³⁴ M. Tatsumisago, Y. Shinkuma, T. Saito, and T. Minami, *Solid State Ionics* **50**, 273 (1992).
 - ³⁵ C. Rousselot, J. P. Malugani, R. Mercier, M. Tachez, P. Chieux, A. P. Pappin, and M. D. Ingram, *Solid State Ionics* **78**, 211 (1995).
 - ³⁶ M. Villa, G. Chiodelli, A. Magistris, and G. J. Licheri, *J. Chem. Phys.* **85**, 2392 (1986).
 - ³⁷ S. Martin, H. Bischoff, M. Mali, J. Ross, and D. Brinkmann, *Solid State Ionics* **18-19**, 421 (1986).
 - ³⁸ S. H. Chung, K. R. Jeffrey, J. R. Stevens, and L. Borjesson, *Phys. Rev. B* **41**, 6154 (1990).
 - ³⁹ H. L. Tuller and D. P. Button, in *Transport-Structure Relations in Fast Ion and Mixed Conductors*, edited by F. W. Poulsen, N. Hessel-Anderson, K. Clausen, S. Skaarup, and O. Soerensen (Risø National Laboratory, Roskilde, Denmark, 1985), p. 119.
 - ⁴⁰ J. Swenson and L. Borjesson, *Phys. Rev. Lett.* **77**, 3569 (1996).
 - ⁴¹ K. Terashima, T. Hashimoto, and T. Yoko, *Phys. Chem. Glasses* **37**, 129 (1996).
 - ⁴² G. Chiodelli, A. Magistris, M. Villa, and J. L. Bjorkstam, *J. Non-Cryst. Solids* **51**, 143 (1982).
 - ⁴³ F. Rocca, G. Dalba, P. Fornasini, and A. Tomasi, *Solid State Ionics* **53-56**, 1253 (1992).
 - ⁴⁴ G. Licheri, A. Musinu, G. Paschina, G. Piccaluga, G. Pinna, and A. Magistris, *J. Chem. Phys.* **85**, 500 (1986).
 - ⁴⁵ A. Fontana and F. Rocca, *Phys. Rev. B* **36**, 9279 (1987).
 - ⁴⁶ E. I. Kamitsos, J. A. Kapoutsis, G. D. Chryssikos, and A. P. Patsis, *Bol. Soc. Esp. Ceram. Vidrio*, **31-C4** 403 (1992).
 - ⁴⁷ E. I. Kamitsos, J. A. Kapoutsis, G. D. Chryssikos, J. M. Hutchinson, A. J. Pappin, M. D. Ingram, and J. A. Duffy, *Phys. Chem. Glasses* **36**, 141 (1995).
 - ⁴⁸ J. J. Hudgens and S. W. Martin, *Phys. Rev. B* **53**, 5348 (1996).
 - ⁴⁹ M. Hanaya, M. Nakayama, A. Hatate, and M. Oguni, *Phys. Rev. B* **52**, 3234 (1995).
 - ⁵⁰ M. Tatsumisago, N. Itakura, and T. Moinami, *J. Non-Cryst. Solids* **232-234**, 267 (1998).
 - ⁵¹ J. Swenson, L. Borjesson, R. L. McGreavy, and W. S. Howells, *Phys. Rev. B* **55**, 11 236 (1997).
 - ⁵² L. Cervinka, F. Rocca, P. Fornasini, and G. Dalba, *J. Non-Cryst. Solids* **150**, 140 (1992).
 - ⁵³ L. Cervinka, J. Bergorova, A. Damaso, and F. Rocca, *J. Non-Cryst. Solids* **232-234**, 627 (1998).
 - ⁵⁴ C. Liu and C. A. Angell, *J. Chem. Phys.* **93**, 7378 (1990).
 - ⁵⁵ C. P. Varsamis, E. I. Kamitsos, N. Machida, and T. Minami, *J. Phys. Chem. B* **101**, 3734 (1997).
 - ⁵⁶ E. I. Kamitsos, Y. D. Yiannopoulos, C. P. Varsamis, and H. Jain, *J. Non-Cryst. Solids* **222**, 59 (1977).

- ⁵⁷E. I. Kamitsos, Y. D. Yiannopoulos, H. Jain, and W. C. Huang, *Phys. Rev. B* **54**, 9775 (1996).
- ⁵⁸S. Cunsolo, P. Dore, and C. P. Varsamis, *Appl. Opt.* **31**, 4554 (1992).
- ⁵⁹(a) E. I. Kamitsos, A. P. Patsis, M. A. Karakassides, and G. D. Chryssikos, *J. Non-Cryst. Solids* **126**, 52 (1990); (b) E. I. Kamitsos, A. P. Patsis, and G. D. Chryssikos, *ibid.* **152**, 246 (1993).
- ⁶⁰J. A. Kapoutsis, E. I. Kamitsos, and G. D. Chryssikos, in *Borate Glasses, Crystals and Melts*, edited by A. C. Wright, S. A. Feller, and A. C. Hannon (Society of Glass Technology, Sheffield, UK, 1997), p. 303.
- ⁶¹J. L. Piguet and J. E. Shelby, *J. Am. Ceram. Soc.* **68**, 450 (1985).
- ⁶²S. D. Ross, *Inorganic Infrared and Raman Spectra* (McGraw-Hill, New York, 1972), p. 260.
- ⁶³J. C. Manificier, J. Gasiot, and J. P. Fillard, *J. Phys. E* **9**, 1002 (1976).
- ⁶⁴K. S. Kim and P. J. Bray, *J. Nonmet.* **2**, 95 (1974).
- ⁶⁵J. Krogh-Moe, *Phys. Chem. Glasses* **6**, 46 (1965).
- ⁶⁶E. I. Kamitsos and G. D. Chryssikos, *J. Mol. Struct.* **247**, 1 (1991).
- ⁶⁷K. Nakamoto, *Infrared and Raman Spectra of Inorganic and Coordination Compounds* (Wiley, New York, 1978), p. 127.
- ⁶⁸R. J. Araujo, *J. Non-Cryst. Solids* **58**, 201 (1983).
- ⁶⁹S. Sen, Z. Xu, and J. F. Stebbins, *J. Non-Cryst. Solids* **226**, 29 (1998).
- ⁷⁰A. Karki, S. Feller, P. Lim, J. Stark, C. Sanchez, and M. Shibata, *J. Non-Cryst. Solids* **92**, 11 (1987).
- ⁷¹G. Brachtel and M. Jansen, *Z. Anorg. Allg. Chem.* **478**, 13 (1981).
- ⁷²M. Jansen and G. Brachtel, *Z. Anorg. Allg. Chem.* **489**, 42 (1981).
- ⁷³G. Dalba, P. Fornasini, F. Rocca, E. Bernieri, E. Burattini, and S. Mobilio, *J. Non-Cryst. Solids* **91**, 153 (1987).
- ⁷⁴J. Krogh-Moe, *Acta Crystallogr.* **18**, 77 (1965).
- ⁷⁵E. I. Kamitsos and G. D. Chryssikos, *Solid State Ionics* **105**, 75 (1998).
- ⁷⁶G. L. Bottger and A. L. Geddes, *J. Chem. Phys.* **46**, 3000 (1967).
- ⁷⁷G. Burns, F. H. Dacol, and M. W. Shafer, *Phys. Rev. B* **16**, 1416 (1977).
- ⁷⁸E. I. Kamitsos, *J. Phys. Chem.* **93**, 1604 (1989).